SCIENCE CHINA
Chemistry

• ARTICLES •

February 2018 Vol.61 No.2: 206–214
https://doi.org/10.1007/s11426-017-9133-5

# Side-chain fluorination on the pyrido[3,4-*b*]pyrazine unit towards efficient photovoltaic polymers

Tao Wang[1,2], Liuliu Feng[1], Jun Yuan[1], Lihui Jiang[1], Wei Deng[2], Zhi-Guo Zhang[3], Yongfang Li[3] & Yingping Zou[1*]

[1]*College of Chemistry and Chemical Engineering, Central South University, Changsha 410083, China*
[2]*State Key Laboratory of Chemo/Biosensing and Chemometrics, Hunan University, Changsha 410082, China*
[3]*Beijing National Laboratory for Molecular Sciences, Institute of Chemistry, Chinese Academy of Sciences, Beijing 100190, China*

Received July 27, 2017; accepted August 29, 2017; published online December 15, 2017

A series of new polymer donors (PT-PP, PT-2*f*PP and PT-4*f*PP) were synthesized based on alkylthiophene substituted benzodithiophene (BDT-T) and pyrido[3,4-*b*]pyrazine (PP) building blocks and the effects of fluorination on the polymer properties were explored. Photophysical properties, charge mobilities and morphologies of the three polymers have been intensively investigated. The results indicated that the introduction of the fluorine atom at meta-positions of phenyl substituted PP unit hardly affected their highest occupied molecular orbital (HOMO) level. More importantly, controlling the degree of side-chain fluorination in the polymers is crucial for optimizing the blend morphology. Three polymers showed different photovoltaic properties. The polymer solar cell (PSC) based on the single layer device structure of ITO/PEDOT:PSS/PT-4*f*PP:$PC_{71}BM$ (1:1, *w*:*w*)/ZrAcac/Al demonstrates a high power conversion efficiency (PCE) of 7.61% under the illumination of AM 1.5G, 100 mW $cm^{-2}$, which is the highest value for PP-based PSCs.

**side-chain fluorination, pyrido[3,4-*b*]pyrazine, efficient photovoltaics**

**Citation:** Wang T, Feng L, Yuan J, Jiang L, Deng W, Zhang ZG, Li Y, Zou Y. Side-chain fluorination on the pyrido[3,4-*b*]pyrazine unit towards efficient photovoltaic polymers. *Sci China Chem*, 2018, 61: 206–214, https://doi.org/10.1007/s11426-017-9133-5

## 1 Introduction

Solution-processed polymer solar cells (PSCs) have been intensively investigated in recent years due to several advantages such as lightweight, low-cost, mechanical flexibility and roll-to-roll solution processability [1–3]. Up to now, the bulk-heterojunction (BHJ) PSC has become one of the most successful device structures developed in the field. Conjugated polymers and fullerene derivatives (such as [6,6]-phenyl-$C_{61}$(or $C_{71}$)-butyric acid methyl ester ($PC_{61}BM$ or $PC_{71}BM$)) have been widely used as the electron donor and acceptor materials, respectively [4]. The highest power conversion efficiencies (PCEs) of BHJ PSCs have been dramatically improved to over 11% [5–7], due to the development of new donor materials [8], engineered interfaces and enhanced control of polymeric film microstructure [9]. Further improvement of PCE is still required for commercialization. As well known, the influencing factors of PCE include the open-circuit voltage ($V_{oc}$), the short-circuit current density ($J_{sc}$) and the fill factor (FF). In order to obtain high performance polymer solar cells, it is important to design new electron-donating polymer materials that should possess the following features: (1) a broad and strong absorption for ensuring efficient harvest sunlight; (2) low-lying highest occupied molecular orbital (HOMO) level and appropriate lowest unoccupied molecular orbital (LUMO) level for keeping efficient charge separation with low energy loss; (3)

*Corresponding author (email: yingpingzou@csu.edu.cn)

high charge mobilities. It is difficult to design a conjugated polymer to satisfy all these requirements [3,10,11]. Therefore, it is of great interest to design appropriate pairs of donor and acceptor polymers with complementary light absorption and suitable energy levels to maximize $J_{sc}$, FF and $V_{oc}$ values simultaneously.

As demonstrated in earlier studies on PSCs, the development of conjugated polymers with alternating electron-rich donor (D) and electron-poor acceptor (A) building units is a universal strategy for preparing high efficiency donor materials, since D-A copolymers can facilitate the fine-tuning of absorption bands and charge transporting properties, etc [12–15]. Therefore, the design of new donor and acceptor building motifs has always been one of the most important research works to construct D-A copolymers for high efficient PSCs. So far, several types of electron-withdrawing units have been identified, including 2,1,3-benzothiadiazole (BT) [16–18], thienothiophene (TT) [19–22] and quinoxaline (Qx) [23–25]. They have been developed to build conjugated D-A copolymers in PSCs with excellent photovoltaic properties. Recently, it also has been found that the introduction of some unsymmetrical conjugated building blocks into conjugated backbones may significantly improve the device performance [26,27]. Nitrogen atom has been frequently utilized to replace carbon atom as electron-deficiency moieties to optimize the photoelectric properties [28,29], which may help form a comprehensive understanding on the structure-property relationships. By replacing the benzene ring of dibenzo[*a*,*c*]phenazine (BPz) [30,31], Qx, 2H-benzo[*d*][1,2,3]triazole (BTz) [32,33], and BT with pyridine, [1,2,5]thiadiazolo[3,4-*c*]pyridine (PT) [34], dibenzo[*f*,*h*]pyrido [3,4-*b*]quinoxaline (BPQ) [35], pyrido[3,4-*b*]pyrazine (PP) [36,37], and 2H-[1,2,3]triazolo[4,5-*c*]pyridine (TP) become electron-deficiency moieties and can be utilized for the design of low-bandgap (LBG) materials with low HOMO energy level. Among a wide variety of unsymmetrical acceptor units, PP unit is an easily synthesized and promising electron-deficient unit for optoelectronic applications. It has already been widely utilized in NIR light-emitting diodes, field-effect transistors, two-photon absorption and BHJ solar cells [38]. Some PP-based conjugated polymers have been described previously [35,36,39], these PP-based conjugated polymers have shown higher electron-accepting abilities relative to that of Qx-based conjugated polymers due to the former structure more electron-withdrawing nitrogen atoms in the pyridine ring (see Scheme 1) [39]. Furthermore, the PP motif can provide the versatility of introducing different substituents easily on the 2 and 3 positions, which could be used to tune the solubility, bandgap and energy levels of the resulting polymers. As well known, 2,3-diphenylpyrido[3,4-*b*]pyrazine, which possesses two separated phenyl rings, is one of the commonly investigated PP derivatives because of its facile synthesis and versatility. Thus, using the PP unit as components in PSCs is an efficient way to improve the PCE. To date, only a few D-A PP-based conjugated polymers were synthesized for photovoltaic applications. Some studies indicated that PP-based polymers as light-harvesting and electron-donating materials have exhibited poor PCEs (less than 6.2% [40]). The low efficiency is probably due to the low molecular weights, poor solubility and the non-planar nature of the two pendent phenyl groups attached on PP, leading to poor interchain packing and thus to suppress hole mobility, which partially limits the further development of PP-based conjugated polymers [39]. Based on the above reasons, PP-based conjugated polymers received less attention compared to those from their similar counterpart-Qx-based polymers. On the other hand, benzo[1,2-*b*:4,5-*b*′]-dithiophene (BDT) is one of the most excellent electron donor units for photovoltaic applications due to its desirable peculiarities such as structural rigidity and planarity, favorable inter-chain π-π stacking and the presence of additional substitution sites for the incorporation of side chains [41,42]. Recently, fluorination of conjugated polymers has been demonstrated as a highly effective approach for optimizing optical and electrical properties, thereby enhancing the photovoltaic performance of fullerene-based PSCs. Since the size of fluorine is small, which can minimize the undesired steric interactions. Meanwhile, the introduction of fluorine atoms on the conjugated polymers can promote the molecular planarity and intermolecular assembly due to the C-F and F-H in the polymer, resulting in a better charge mobility of the polymers [43]. Furthermore, fluorination can also improve BHJ morphology with smaller phase domains and larger interfacial areas that increase the exciton dissociation [44,45]. As a result, the FF and $J_{sc}$ of the corresponding devices are improved. Therefore, developing new methods to utilize the fluorination more effectively is of great importance to design conjugated polymer for the photovoltaic applications.

Prompted by the above mentioned considerations, to this end, we developed three new p-type PP-based polymers, PT-PP, PT-2*f*PP, and PT-4*f*PP, three target copolymers are based on phenyls substituted PP acceptor units M1, M2, M3 and BDT-T donor unit M4. The synthetic routes of PT-PP, PT-2*f*PP, and PT-4*f*PP are shown in Figure 1. The effects of fluorination on the photovoltaic performances were investigated. It is different from the previous work that

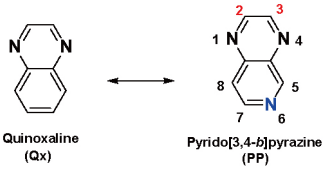


**Scheme 1** Chemical structures of the quinoxaline (Qx) and pyrido[3,4-*b*]pyrazine (PP) (color online).

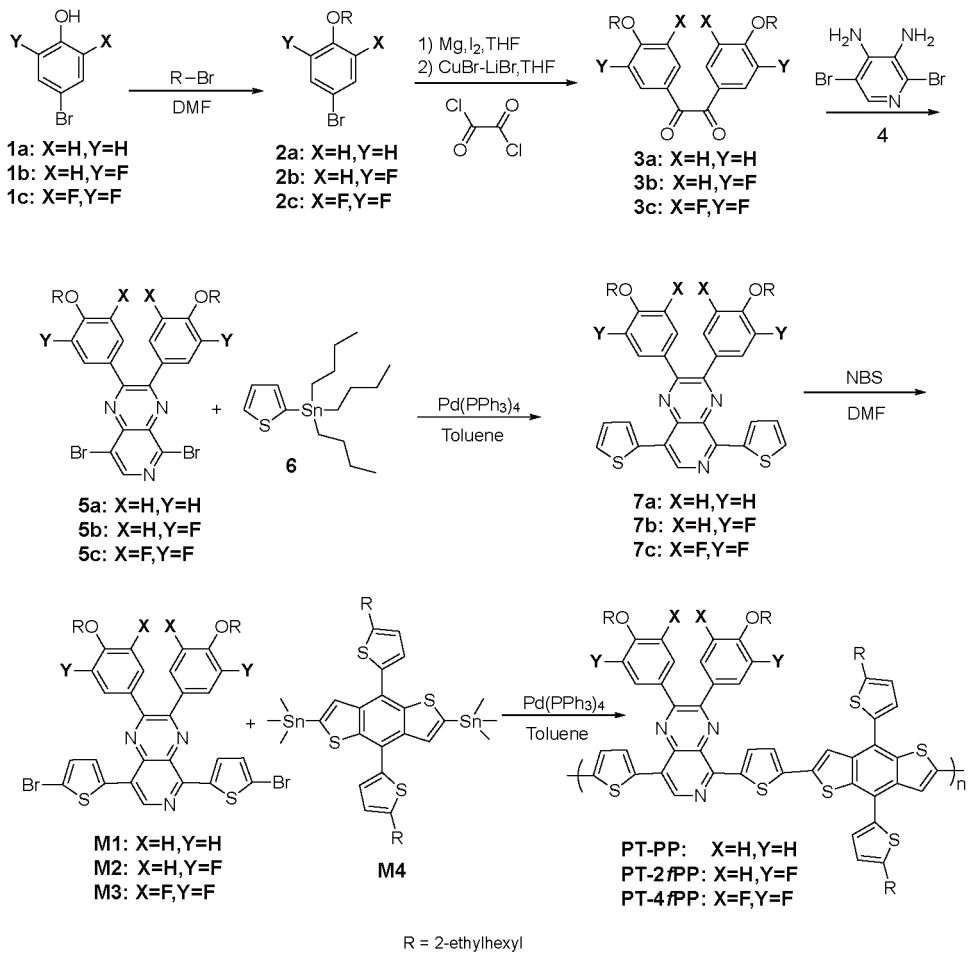


**Figure 1** Synthetic routes for the monomers and the corresponding polymers.

introduced the fluorine atom into the backbone of polymer chains, we introduced diverse numbers and different positions of fluorine atoms into the side-chain of the polymer acceptor units and systematically explored the effects of the side-chain fluorination on the fullerene-based PSC performances. Side-chain engineering is indeed an essential and widespread technique to tune the optophysical properties of a conjugated polymer to achieve high performance PSCs, including absorption, energy level, molecular packing and charge transport [46]. Side-chain fluorination of the polymers had a remarkable impact on the device performance: the PCEs increase from 4.44% for the PT-PP- to 5.53% and 7.61% for the PT-2*f*PP- and PT-4*f*PP-based fullerene PSCs, respectively. The introduction of fluorine atoms onto phenyl away from the polymer backbone benefit enhancing absorption coefficients and promoting exciton dissociations with suppressed recombination processes, thereby, leading to a higher $J_{sc}$ and FF values. Moreover, the side-chain fluorination of polymers facilitated the formation of better BHJ morphology with well-intermixed blend domains. Obviously, the degree of fluorination had important influence on the performances of the fullerene PSCs. For example, the best efficiency was achieved by the PT-4*f*PP (7.61%) device more than the PT-PP (4.44%) and PT-2*f*PP (5.53%) device due to increased electronic properties, including high charge mobilities, higher balanced hole/electron mobilities ($\mu_h/\mu_e$) ratio and better charge dissociation. To the best of our knowledge, the PCE of 7.61% is the highest value reported in literatures to date for the PP-based photovoltaic polymers.

## 2 Results and discussion

### 2.1 Synthesis of the polymers

As shown in Figure 1, the polymers were prepared by the typical Stille-couping polymerization reaction between the BDT-T monomer (M4) and the M1, M2 or M3 monomer. Three polymers were synthesized with the same conditions, i.e., using toluene as solvent and tetrakis(triphenylphosphine)palladium (**0**) $Pd(PPh_3)_4$ as catalyst; the polymerizations were taken at 110 °C under inert atmosphere for 24 h. The crude polymers were precipitated into methanol and filtered. After that, they were subjected to Soxhlet extraction successively with methanol, hexane, acetone and

chloroform. Then chloroform fractions were concentrated under vacuum evaporation, precipitated into methanol and collected by filtration. The detailed synthesis process and structural characterization of PT-PP, PT-2*f*PP, and PT-4*f*PP are described in the supporting information (see supporting information online). The molecular weight of the polymers was estimated by high-temperature gel permeation chromatography (HT-GPC) using 1,2,4-tricholorobenzene as the eluent at 150 °C and monodispersed polystyrene as the standard. For PT-PP, PT-2*f*PP, and PT-4*f*PP, the number-average molecular weight ($M_n$) is 11.3, 13.2, and 12.9 kDa, and the polydispersity index (PDI) is 2.33, 1.79, and 1.9. According to the results from thermogravimetric analysis (TGA), the decomposition onset temperatures ($T_d$) of these polymers are all above 280 °C (Figure S10, see Supporting Information online). The related data including the molecular weight and TGA of these three polymers are listed in Table 1.

### 2.2 Optical absorption properties and photoluminescence characteristics

Ultraviolet-Visible (UV-Vis) absorption spectra of the polymers in a dilute chloroform solution and thin films at 25 °C are shown in Figure 2(a,b), and the characteristics of the polymers absorption are summarized in Table 1. Three polymers showed similar absorption profiles with three major peaks with different absorption maxima and an obvious red-shift from solution to film due to the aggregation of the conjugated main chain in the solid state. The higher energy band in the wavelength range of 300–500 nm arises from the localized π-π transition, whereas a relatively broad and weak absorption in the wavelength range of 500–750 nm can be attributed to the intramolecular charge transfer (ICT) between the strong electron-accepting fluorinated or non-fluorinated PP units and electron-donating BDT units. Compared with the solutions, PT-PP, PT-2*f*PP, and PT-4*f*PP are red-shifted by ca. 13, 2, and 13 nm, respectively, in the film states, indicating that there are aggregations of polymer backbone and π-π intermolecular interactions in the solid film states. In solid thin films, the absorption edges of PT-PP, PT-2*f*PP, and PT-4*f*PP are 723, 762, and 773 nm, corresponding to optical bandgaps ($E_g^{opt}$=1240/$\lambda_{edge}$) of 1.72, 1.63, and 1.60 eV, respectively, implying that the introduction of fluorine atoms at different positions of the side-chian has a significant influence on the bandgaps of the polymers. The extinction coefficients of the polymers in thin film ($\varepsilon_{film}$) were measured (as shown in Figure S11) and listed in Table 1. As for polymer thin films, PT-4*f*PP showed the highest extinction coefficient ($\varepsilon_{film}$=4.1×10$^4$ cm$^{-1}$), while the polymer PT-PP showed the lowest extinction coefficient ($\varepsilon_{film}$=3.5×10$^4$ cm$^{-1}$). The improvement of extinction coefficient is probably due to the auxochromic effect of fluorine atom. In order to further investigate the exciton dissociation and charge transfer behavior, photoluminescence (PL) quenching experiments were conducted in the blend films. From the PL spectra in Figure 2(c–e), it is clear that the spectral shape of pure polymers are broad. PL emission peaks of the fluorinated polymers appeared in the range of 700–850 nm centered at 820 nm, however, PT-PP centered at 720 and 820 nm. For the blend films, their emissions were almost all quenched (by over 90%), suggesting effective electron transfer from the polymers to $PC_{71}BM$ for the excitons generated in the donor phase.

### 2.3 Electrochemical properties

The molecular energy levels of three polymers were examined by cyclic voltammetry (CV) measurements (Figure 3(a)), and the energy levels are shown in Figure 3(b). The polymer film was prepared by drop casting the polymer dissolved in chloroform on the electrode. Measurements were performed with Ag/AgCl as the reference electrode in anhydrous acetonitrile ($CH_3CN$) solution of 0.1 M of tetrabuylammonium hexafluorophosphate ($Bu_4NPF_6$). The oxidation onset potentials ($E_{ox}^{onset}$) of PT-PP, PT-2*f*PP and PT-4*f*PP are 0.94, 0.84, and 0.85 V, respectively. The onset potentials for reduction ($E_{red}^{onset}$) of them were found to be −0.96, −0.86, and −0.81 V, respectively. The HOMO and the LUMO energy levels of the polymers can be calculated according to the following equations: HOMO=−$e$($E_{ox}^{onset}$+4.41) (eV) and LUMO=−$e$($E_{red}^{onset}$+4.41) (eV), where the unit of $E_{ox}^{onset}$ and $E_{red}^{onset}$ is in *vs*. Ag/AgCl [46]. The HOMO levels of PT-PP, PT-2*F*pp, and PT-4*f*PP are −5.35, −5.25, and −5.26 eV, respectively, and their LUMO levels are −3.45, −3.55, and −3.60 eV, respectively. Notably, compared to the fluorinated polymers (PT-2*f*PP and PT-4*f*PP), PT-PP shows a lower HOMO level, implying that the introduction of fluorine atom at the phenyl away from the conjugated backbone has little influence on the HOMO energy level of the

**Table 1** Optical parameters and physical properties of the polymers

| Polymer | sol $\lambda_{max}$ (nm)[a)] | sol $\lambda_{edge}$ (nm)[a)] | film $\lambda_{max}$ (nm)[b)] | film $\lambda_{edge}$ (nm)[b)] | $E_g^{opt}$ (eV) | $\varepsilon_{film}$ ($10^4$) ($cm^{-1}$) | $M_n$ (kDa) | PDI | $T_d$ (°C)[c)] |
|---|---|---|---|---|---|---|---|---|---|
| PT-PP | 585 | 701 | 598 | 723 | 1.72 | 3.5 | 11.3 | 2.33 | 284 |
| PT-2*f*PP | 639 | 753 | 641 | 762 | 1.63 | 3.6 | 13.2 | 1.79 | 295 |
| PT-4*f*PP | 650 | 766 | 663 | 773 | 1.60 | 4.1 | 12.9 | 1.90 | 354 |

a) Measured in chloroform solution; b) cast from chloroform solution; c) decomposition temperature at 5% weight loss

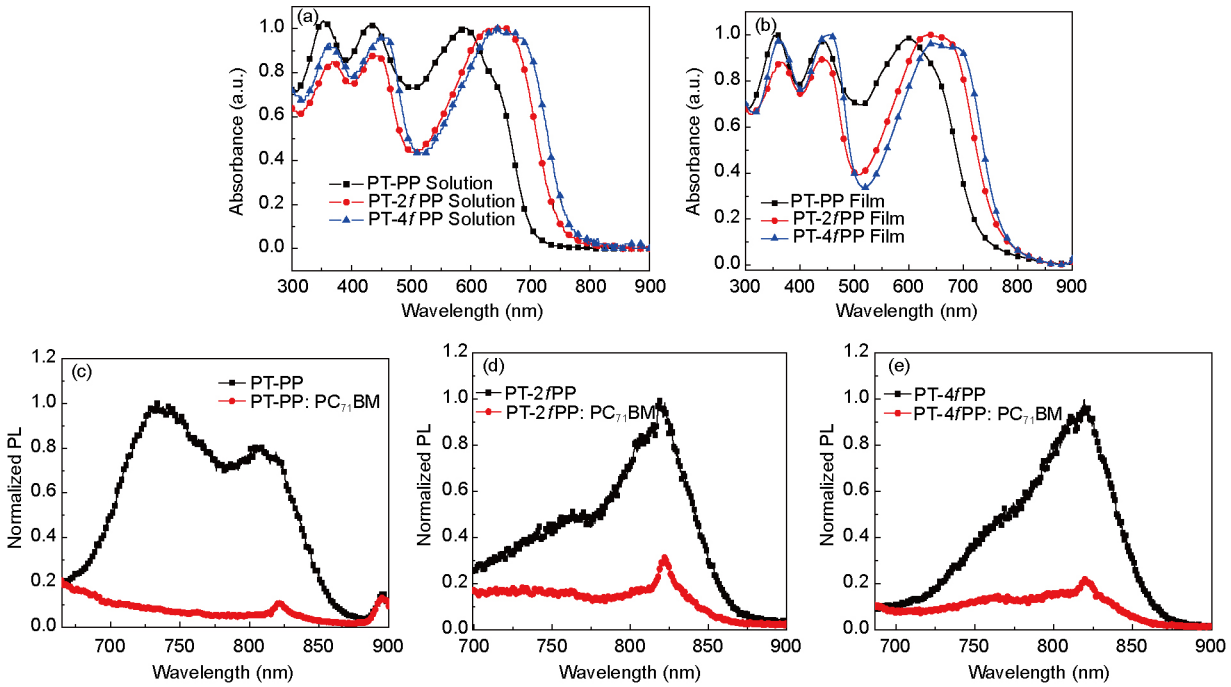


**Figure 2** UV-Vis absorption spectra of PT-PP, PT-2*f*PP, and PT-4*f*PP in chloroform solution (a) and in the thin solid film (b) at 25 °C; (c–e) photoluminescence spectra of pure PT-PP, PT-2*f*PP, and PT-4*f*PP as well as blend films of PT-PP:$PC_{71}BM$, PT-2*f*PP:$PC_{71}BM$, and PT-4*f*PP:$PC_{71}BM$ (color online).

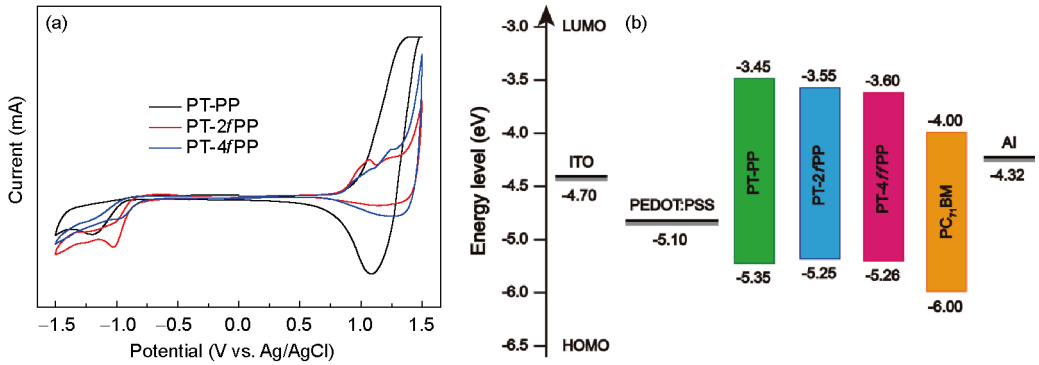


**Figure 3** (a) Cyclic voltammograms of PT-PP, PT-2*f*PP, and PT-4*f*PP in 0.1 M $Bu_4NPF_6$ $CH_3CN$ solution at a scan rate of 50 mV $s^{-1}$ and (b) energy levels of PT-PP, PT-2*f*PP, and PT-4*f*PP (color online).

polymer. This highlighted the importance of our molecular design of the side-chain fluorination, which was different from the other backbone fluorinations that often induced the changes in the bandgaps [47–50]. The electrochemical bandgaps ($E_g^{CV}$) of the polymers calculated from the difference between HOMO and LUMO values, were 1.90, 1.70, and 1.66 eV for PT-PP, PT-2*f*PP and PT-4*f*PP, respectively. The $E_g^{CV}$ are slightly larger than the optical bandgaps. This discrepancy might have been induced by the presence of an energy barrier at the interface by the polymer film and the electrode surface [51]. The CV data of polymers are summarized in Table 2.

**Table 2** Redox potentials and energy levels of polymers PT-PP, PT-2*f*PP, and PT-4*f*PP

| Polymer | $E_{ox}^{onset}$(V) | $E_{red}^{onset}$(V) | HOMO (eV)[a)] | LUMO (eV)[a)] | $E_g^{CV}$(eV) |
|---|---|---|---|---|---|
| PT-PP | 0.94 | −0.96 | −5.35 | −3.45 | 1.90 |
| PT-2*f*PP | 0.84 | −0.86 | −5.25 | −3.55 | 1.70 |
| PT-4*f*PP | 0.85 | −0.81 | −5.26 | −3.60 | 1.66 |

a) HOMO=$-e(E_{ox}^{onset}+4.41)$ (eV), LUMO=$-e(E_{red}^{onset}+4.41)$ (eV) using Ag/AgCl as the reference electrode

### 2.4 Photovoltaic properties

The fluorination effect on the photovoltaic properties of PSCs was explored by evaluating PT-PP:$PC_{71}BM$, PT-2*f*PP:$PC_{71}BM$, and PT-4*f*PP:$PC_{71}BM$ based PSCs. BHJ PSCs with a conventional device structure of indium tin oxide (ITO)/poly(3,4-ethylenedioxythiophene)poly(styrenesulfonate) (PEDOT:PSS)/polymer:$PC_{71}BM$/zirconium acetylacetonate (ZrAcac)/Al (100 nm) were fabricated, where PT-PP, PT-2*f*PP, or PT-4*f*PP used as polymer donors, $PC_{71}BM$ is used as electron acceptor, PEDOT:PSS used the hole transport layer (HTL), ZrAcac is used as an electron transport layer (ETL). The active layer was spin-coated from chloroform solution of the polymer donor and $PC_{71}BM$ acceptor. We found that for the devices based on three polymers, the optimal D-A ratios (polymer:$PC_{71}BM$) are 1:1 (as shown in Table S1, see supporting information online). To optimize the morphology of the blend films and thus to enhance photovoltaic performance, 0.3% (or 0.5%) 1,8-diiodooctane (DIO) (*v*/*v*, DIO/chloroform) was added into the solutions of the active layer prior to the spin-coating process. The typical current density-voltage (*J*-*V*) characteristic curves of PSCs under AM 1.5G illumination are shown in Figure 4(a) and related photovoltaic data are listed in Table 3. The detailed photovoltaic properties are shown in Table S1. The PSC based on PT-4*f*PP:$PC_{71}BM$ (1:1, *w*:*w*) using 0.5% DIO as an additive exhibited the best performance with a maximal PCE of 7.61% with a $V_{oc}$ of 0.81 V, a $J_{sc}$ of 14.53 mA cm$^{-2}$ and a FF up to 65% was achieved. Additionally, the PCE of 7.61% is the highest value reported in literatures to date for PP-based PSCs. Compared with the non-fluorinated polymer, PT-PP, the $J_{sc}$ values were increased

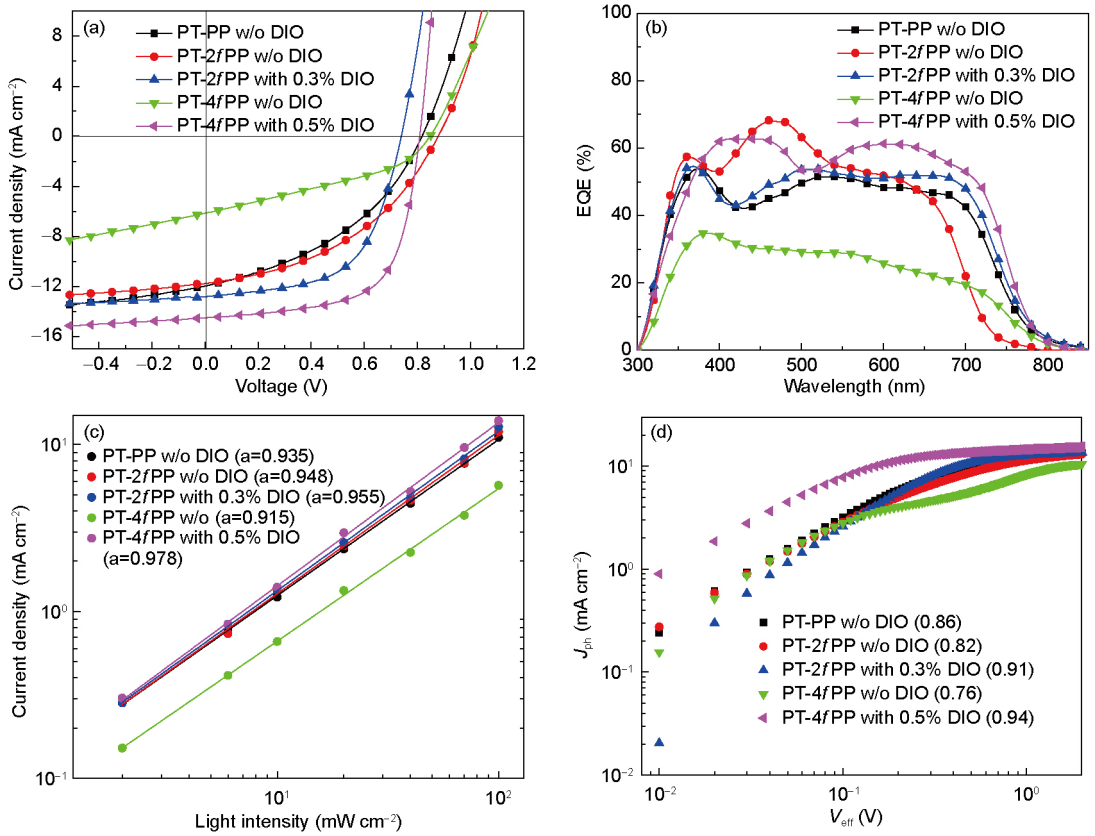


**Figure 4** (a) *J*-*V* curves of the devices of PT-PP, PT-2*f*PP, and PT-4*f*PP with a D-A ratio of 1:1 (polymer:$PC_{71}BM$, *w*:*w*), processed without and with the use of optimum amount of DIO; (b) the EQE curves of single-junction PSC devices with a structure of ITO/PEDOT:PSS/polymer:$PC_{71}BM$/ZrAcac/Al under the illumination of AM 1.5G, 100 mW cm$^{-2}$; (c) plots of $J_{sc}$ versus light intensity; (d) $J_{ph}$ versus $V_{eff}$ plots (color online).

**Table 3** The optimized photovoltaic properties of the PSCs based on polymer:$PC_{71}BM$ (1:1, *w*:*w*) using 0.3% (or 0.5%) DIO under illumination of AM 1.5 G, 100 mV cm$^{-2}$

| Active layer | DIO additive | $V_{oc}$ (V) | $J_{sc}$ (mA cm$^{-2}$) | FF (%) | PCE (%) | Thickness(nm)[a] |
|---|---|---|---|---|---|---|
| PT-PP/$PC_{71}BM$ | w/o | 0.88 (0.86±0.02) | 11.8 (11.3±0.5) | 43 (42±1) | 4.44 [4.08] | 85 |
| PT-2*f*PP/$PC_{71}BM$ | 0.3% | 0.74 (0.73±0.01) | 12.8 (12.6±0.2) | 58 (56±2) | 5.53 [5.15] | 105 |
| PT-4*f*PP/$PC_{71}BM$ | 0.5% | 0.81 (0.80±0.01) | 14.5 (14.4±0.1) | 65 (64±1) | 7.61 [7.37] | 95 |

a) thickness of the active layers

by 1.06 and 2.76 mA cm$^{-2}$ for PT-2*f*PP and PT-4*f*PP based PSCs. The results indicate that molecular modification by introducing fluorine atoms at the 3(3′)-position of phenyl onto PP unit will be a promising strategy to decrease the LUMO level and increase the extinction coefficient of the conjugated polymers, and further enhancing the photovoltaic performance of PSCs. Meanwhile, the higher FF is benefited from improved carrier mobility due to the introduction of fluorine.

To verify the accuracy of the measurement of the devices, the corresponding external quantum efficiency (EQE) curves of the aforementioned five devices are shown in Figure 4(b) [52]. The EQE profiles from the polymer:$PC_{71}BM$ blends are consistent with their corresponding absorption spectra (Figures 2(a, b)). By the use of 0.5% DIO as a solvent additive, the PT-4*f*PP-based device exhibited quite efficient EQE responses from 350 to 700 nm and the maximum EQE plateau reaches 50% from 370 to 700 nm. According to the EQE curves, the calculated $J_{sc}$ values of the devices agree well with $J_{sc}$ from *J*-*V* measurements within 5% mismatch, indicating that our photovoltaic results are reliable.

In order to gain insight into the effects of the fluorine atom on the device performances, we studied the bimolecular recombination kinetics of the active layer in the devices. Figure 4(c) shows the various devices of PT-PP:$PC_{71}BM$, PT-2*f*PP:$PC_{71}BM$ and PT-4*f*PP:$PC_{71}BM$ under different light intensities to study charge recombination under the short circuit condition. In general, $J_{sc}$ has a power-law dependence on light intensity ($P_{light}$) ($J_s \propto P_{light}^{a}$), and power-law component ($a$) value approaches unity when bimolecular recombination is negligible. The $a$ value (0.978) of the PT-4*f*PP blend was closer to unity than those of the PT-PP blend (0.935) and the PT-2*f*PP blend (0.955). Although the differences were not significant, the results indicated that bimolecular recombination was suppressed most effectively in PT-4*f*PP devices. The suppressed recombination correlate well with the higher charge carrier mobilities observed for the PT-4*f*PP:$PC_{71}BM$ and could account partially for the higher FF for the device based on PT-4*f*PP:$PC_{71}BM$.

Next, to further understand the difference of $J_{sc}$ and FF between three polymers, we also measured the photocurrent density ($J_{ph}$) versus the effective voltage ($V_{eff}$) (Figure 4(d)) to investigate the process of excition generation, excition dissociation and carrier collection efficiency [53]. $V_{eff}$ can be defined as $V_{eff}=V_o-V_{bias}$, where $V_o$ is the voltage when $J_{ph}=0$ and $V_{bias}$ is the applied external voltage bias. $J_{ph}$ can be defined as $J_{ph}=J_L-J_D$, where $J_L$ and $J_D$ are the current densities under illumination and in the dark, respectively [54]. At a large reverse voltage (i.e., $V_{eff}>2.4$ V), $J_{ph}$ reaches saturation ($J_{sat}$), meaning that almost all excitions are dissociated into free carriers and rapidly move toward the corresponding electrodes with minimal recombination. Thus, the $J_{ph}/J_{sat}$ ratio can be explained as the exciton dissociation and charge collection efficiency. Compared to the nonfluorinated polymer, high values of 94% and 91% were achieved for PT-2*f*PP:$PC_{71}BM$ and PT-4*f*PP:$PC_{71}BM$, respectively, under the optimal conditions. PT-4*f*PP:$PC_{71}BM$ shows the highest $J_{ph}$ among the three polymer blends, indicating the most efficient charge generation and extraction. The results are in good agreement with the molecular structures, film morphology and photovoltaic properties.

### 2.5 Hole mobility

To further understand the exceptionally high FF of the BHJ PSCs, charge carrier mobilities were measured using space limited current (SCLC) method with the hole only device (ITO/PEDOT:PSS/active layer/Au) and electron only device (ITO/ZnO/active layer/ZrAcac/Al). Figure 5(a, b) show the $J^{1/2}$-$V$ plots of the polymer/$PC_{71}BM$-based devices with or without DIO treatment, the related results are summarized in Table S2. The calculated $\mu_h/\mu_e$ are $2.47\times10^{-4}/2.68\times10^{-4}$ cm$^2$ V$^{-1}$ s$^{-1}$ for PT-4*f*PP:$PC_{71}BM$, $1.65\times10^{-4}/2.10\times10^{-4}$ cm$^2$ V$^{-1}$ s$^{-1}$ for PT-2*f*PP:$PC_{71}BM$, and $8.94\times10^{-5}/1.53\times10^{-4}$ cm$^2$ V$^{-1}$ s$^{-1}$ for PT-PP:$PC_{71}BM$. The higher and balanced $\mu_h$ and $\mu_e$ should be beneficial for high FF and high PCE of the devices based on PT-4*f*PP:$PC_{71}BM$.

### 2.6 Morphological properties of the polymer:$PC_{71}BM$ blends

Tapping-mode atomic force microscopy (AFM) and transmission electron microscopy (TEM) were used to investigate the surface morphology and the internal morphology of the active layer, respectively [55]. All the blend films were prepared under the same conditions with the optimized photovoltaic devices. As shown in Figure 6(a), the blend film of PT-PP:$PC_{71}BM$ shows a surface root mean square (RMS) roughness of 0.89 nm, meanwhile, TEM image shows large polymer and $PC_{71}BM$ aggregation domains, the large bright and dark regions correspond to polymer and $PC_{71}BM$ rich domains, respectively. Figure 6(f) which indicate poor phase separation in the PT-PP:$PC_{71}BM$ blend film. This may be one of the reasons for the much lower FF (43%) for the PT-PP based device. For the blend films based on those two fluorinated polymers and $PC_{71}BM$ without the use of DIO (as shown in Figures 6(b, d)), the RMS roughness of the blend surface is slightly increased. Large-scale phase separation can also be observed (see Figures 6(g, i)). However, with DIO, dramatic changes of the film morphology can be found in two blend films. As observed in Figure 6(j), a fibrillar-like bicontinuous interpenetrating network can be observed. This morphology is beneficial for charge separation and transport, so the high $J_{sc}$ (14.5 mA cm$^{-2}$) and FF (65%) are obtained for PT-4*f*PP based device.

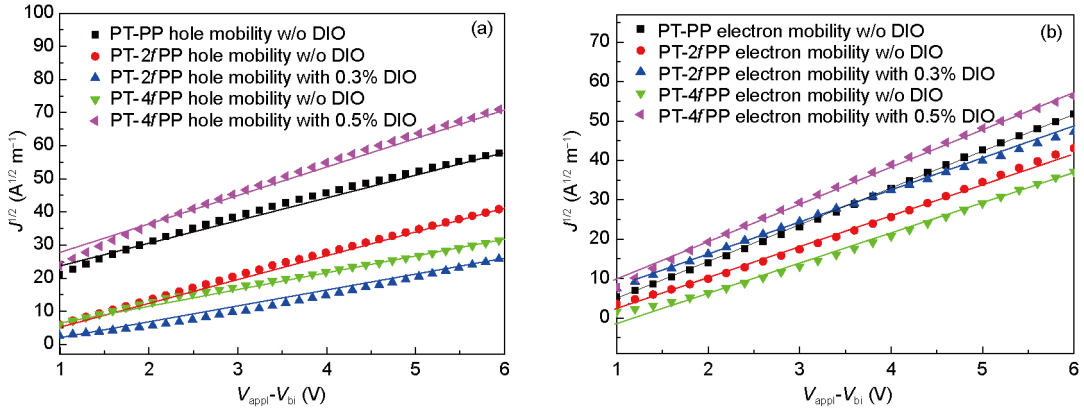


**Figure 5** $J^{1/2}$-$V$ plots of the hole mobility (a) and electron mobility (b) of the polymer:$PC_{71}BM$ (1:1, *w*:*w*), processed without and with the use of optimum amount of DIO (color online).

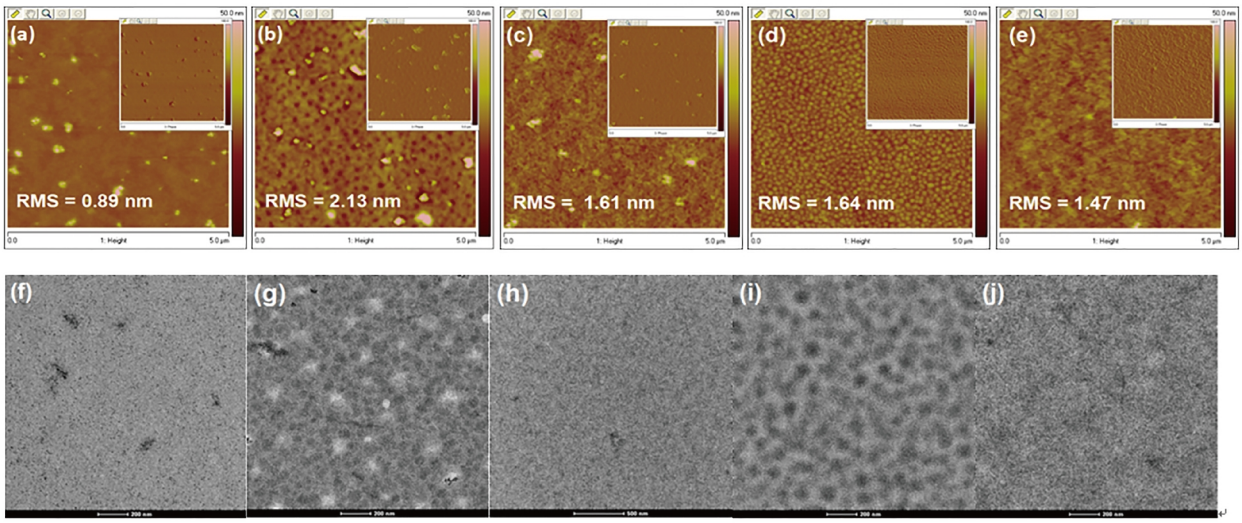


**Figure 6** AFM height images of the active layers of PT-PP:$PC_{71}BM$ (1:1, *w*:*w*) (a), PT-2*f*PP:$PC_{71}BM$ (1:1, *w*:*w*) (b) and with 0.3% DIO (c) and PT-4*f*PP:$PC_{71}BM$ (1:1, *w*:*w*) (d) and with 0.5% DIO (e); TEM images of the active layers of PT-PP:$PC_{71}BM$ (f), PT-2*f*PP:$PC_{71}BM$ (1:1, *w*:*w*) (g) and with 0.3% DIO (h) and PT-4*f*PP:$PC_{71}BM$ (1:1, *w*:*w*) (i) and with 0.5% DIO (j). The AFM (height and phase) image size is 5 μm×5 μm and the scale bar in TEM image is 200 nm (color online).

## 3 Conclusions

In summary, we synthesized a series of new polymer donors (PT-PP, PT-2*f*PP, and PT-4*f*PP) based on BDT-T and PP building blocks and investigated the impacts of fluorination on the polymer properties. The fluorination on the side-chain of conjugated polymers had little influence on thermal stabilities and HOMO energy level, but effectively reduced the LUMO energy level. In addition, side-chain fluorination of the polymers had a remarkable impact on the extinction coefficient and carrier mobility, resulting in high $J_{sc}$ and FF values in BHJ PSCs. More importantly, controlling the degree of side-chain fluorination in the polymers is crucial for optimizing the blend morphology. As a result, when 0.5% DIO was used as a processing additive, for the PT-4*f*PP based device, the PCE got increased to 7.61% from 1.91%, which is the highest for PP-based PSCs with a single heterojunction structure. Therefore, the structural optimization for the number and the position of the fluorine atoms in design of conjugated polymers is important to achieve highly efficient PSCs.

**Acknowledgments** This work was supported by the National Natural Science Foundation of China (51673205, 21506258), National Key Research & Development Projects of China (2017YFA0206600), Hunan Provincial Natural Science Foundation for Distinguished Young Scholars (2017JJ1029), Natural Science Foundation of Hunan Province (2016JJ3134), Project of Innovation-driven Plan in Central South University, China (2016CX035) and the Fundamental Research Funds for the Central Universities of Central South University (2016zzts023).

**Conflict of interest** The authors declare that they have no conflict of interest.

**Supporting information** The supporting information is available online at http://chem.scichina.com and http://link.springer.com/journal/11426. The supporting materials are published as submitted, without typesetting

or editing. The responsibility for scientific accuracy and content remains entirely with the authors.


1 Liu C, Wang K, Gong X, Heeger AJ. *Chem Soc Rev*, 2016, 45: 4825–4846
2 Clarke TM, Durrant JR. *Chem Rev*, 2010, 110: 6736–6767
3 Li Y. *Acc Chem Res*, 2012, 45: 723–733
4 Yan T, Bin H, Yang Y, Xue L, Zhang ZG, Li Y. *Sci China Chem*, 2017, 60: 537–544
5 Lin Y, Zhao F, Wu Y, Chen K, Xia Y, Li G, Prasad SKK, Zhu J, Huo L, Bin H, Zhang ZG, Guo X, Zhang M, Sun Y, Gao F, Wei Z, Ma W, Wang C, Hodgkiss J, Bo Z, Inganäs O, Li Y, Zhan X. *Adv Mater*, 2017, 29: 1604155
6 Yao H, Ye L, Hou J, Jang B, Han G, Cui Y, Su GM, Wang C, Gao B, Yu R, Zhang H, Yi Y, Woo HY, Ade H, Hou J. *Adv Mater*, 2017, 29: 1700254
7 Yu R, Zhang S, Yao H, Guo B, Li S, Zhang H, Zhang M, Hou J. *Adv Mater*, 2017, 29: 1700437
8 Dutta GK, Kim T, Choi H, Lee J, Kim DS, Kim JY, Yang C. *Polym Chem*, 2014, 5: 2540–2547
9 Zhang S, Yang B, Liu D, Zhang H, Zhao W, Wang Q, He C, Hou J. *Macromolecules*, 2016, 49: 120–126
10 Ma Z, Dang D, Tang Z, Gedefaw D, Bergqvist J, Zhu W, Mammo W, Andersson MR, Inganäs O, Zhang F, Wang E. *Adv Energy Mater*, 2014, 4: 1301455
11 Lee HS, Song HG, Jung H, Kim MH, Cho C, Lee JY, Park S, Son HJ, Yun HJ, Kwon SK, Kim YH, Kim BS. *Macromolecules*, 2016, 49: 7844–7856
12 Wang M, Ma D, Shi K, Shi S, Chen S, Huang C, Qiao Z, Zhang ZG, Li Y, Li X, Wang H. *J Mater Chem A*, 2015, 3: 2802–2814
13 Vohra V, Kawashima K, Kakara T, Koganezawa T, Osaka I, Takimiya K, Murata H. *Nat Photon*, 2015, 9: 403–408
14 Yuan J, Qiu L, Xu S, Zhang Z, Li Y, Zou Y. *Org Electron*, 2016, 37: 287–293
15 Lan L, Chen Z, Hu Q, Ying L, Zhu R, Liu F, Russell TP, Huang F, Cao Y. *Adv Sci*, 2016, 3: 1600032
16 Park SH, Roy A, Beaupré S, Cho S, Coates N, Moon JS, Moses D, Leclerc M, Lee K, Heeger AJ. *Nat Photon*, 2009, 3: 297–302
17 Wang N, Chen Z, Wei W, Jiang Z. *J Am Chem Soc*, 2013, 135: 17060–17068
18 Kim JH, Shin SA, Park JB, Song CE, Shin WS, Yang H, Li Y, Hwang DH. *Macromolecules*, 2014, 47: 1613–1622
19 Liang Y, Wu Y, Feng D, Tsai ST, Son HJ, Li G, Yu L. *J Am Chem Soc*, 2008, 131: 56–57
20 Chen HY, Hou J, Zhang S, Liang Y, Yang G, Yang Y, Yu L, Wu Y, Li G. *Nat Photon*, 2009, 3: 649–653
21 Huo L, Zhang S, Guo X, Xu F, Li Y, Hou J. *Angew Chem*, 2011, 123: 9871–9876
22 Cui C, Wong WY, Li Y. *Energ Environ Sci*, 2014, 7: 2276–2284
23 Chen HC, Chen YH, Liu CC, Chien YC, Chou SW, Chou PT. *Chem Mater*, 2012, 24: 4766–4772
24 Yuan J, Qiu L, Zhang Z, Li Y, He Y, Jiang L, Zou Y. *Chem Commun*, 2016, 52: 6881–6884
25 Yuan J, Ouyang J, Cimrová V, Leclerc M, Najari A, Zou Y. *J Mater Chem C*, 2017, 5: 1858–1879
26 Li G, Zhao B, Kang C, Lu Z, Li C, Dong H, Hu W, Wu H, Bo Z. *ACS Appl Mater Interf*, 2015, 7: 10710–10717
27 Liu D, Zhu Q, Gu C, Wang J, Qiu M, Chen W, Bao X, Sun M, Yang R. *Adv Mater*, 2016, 28: 8490–8498
28 Zhou H, Yang L, Price SC, Knight KJ, You W. *Angew Chem*, 2010, 122: 8164–8167
29 Sun Y, Welch GC, Leong WL, Takacs CJ, Bazan GC, Heeger AJ. *Nat Mater*, 2012, 11: 44–48
30 Shi J, Chen J, Chai Z, Wang H, Tang R, Fan K, Wu M, Han H, Qin J, Peng T, Li Q, Li Z. *J Mater Chem*, 2012, 22: 18830–18838
31 Song HJ, Kim DH, Lee EJ, Moon DK. *J Mater Chem A*, 2013, 1: 6010–6020
32 Price SC, Stuart AC, Yang L, Zhou H, You W. *J Am Chem Soc*, 2011, 133: 4625–4631
33 Liu B, Chen X, He Y, Li Y, Xu X, Xiao L, Li L, Zou Y. *J Mater Chem A*, 2013, 1: 570–577
34 Yuan J, Huang X, Dong H, Lu J, Yang T, Li Y, Gallagher A, Ma W. *Org Electron*, 2013, 14: 635–643
35 He R, Yu L, Cai P, Peng F, Xu J, Ying L, Chen J, Yang W, Cao Y. *Macromolecules*, 2014, 47: 2921–2928
36 Yuan MC, Chiu MY, Chiang CM, Wei KH. *Macromolecules*, 2010, 43: 6270–6277
37 Wolf J, Babics M, Wang K, Saleem Q, Liang RZ, Hansen MR, Beaujuge PM. *Chem Mater*, 2016, 28: 2058–2066
38 Ying W, Yang J, Wielopolski M, Moehl T, Moser JE, Comte P, Hua J, Zakeeruddin SM, Tian H, Grätzel M. *Chem Sci*, 2014, 5: 206–214
39 Wu YQ, Chen HC, Yang YS, Chang SH, Wu PJ, Chu YY, Wu CG. *J Polym Sci Part A-Polym Chem*, 2016, 54: 1822–1833
40 Wang T, Jiang L, Yuan J, Feng L, Zhang ZG, Xiang J, Li Y, Zou Y. *Polym Chem*, 2017, 8: 2227–2234
41 Yao H, Ye L, Zhang H, Li S, Zhang S, Hou J. *Chem Rev*, 2016, 116: 7397–7457
42 Ye L, Zhang S, Huo L, Zhang M, Hou J. *Acc Chem Res*, 2014, 47: 1595–1603
43 Xiao S, Zhang Q, You W. *Adv Mater*, 2017, 29: 1601391
44 Dai S, Zhao F, Zhang Q, Lau TK, Li T, Liu K, Ling Q, Wang C, Lu X, You W, Zhan X. *J Am Chem Soc*, 2017, 139: 1336–1343
45 Nguyen TL, Choi H, Ko SJ, Uddin MA, Walker B, Yum S, Jeong JE, Yun MH, Shin TJ, Hwang S, Kim JY, Woo HY. *Energy Environ Sci*, 2014, 7: 3040–3051
46 Zhang ZG, Li Y. *Sci China Chem*, 2015, 58: 192–209
47 Yuan J, Xiao L, Liu B, Li Y, He Y, Pan C, Zou Y. *J Mater Chem A*, 2013, 1: 10639–10645
48 Zhang M, Guo X, Zhang S, Hou J. *Adv Mater*, 2014, 26: 1118–1123
49 Zheng Z, Awartani OM, Gautam B, Liu D, Qin Y, Li W, Bataller A, Gundogdu K, Ade H, Hou J. *Adv Mater*, 2017, 29: 1604241
50 Xu S, Feng L, Yuan J, Zhang ZG, Li Y, Peng H, Zou Y. *ACS Appl Mater Interf*, 2017, 9: 18816–18825
51 Li Y, Cao Y, Gao J, Wang D, Yu G, Heeger AJ. *Synth Met*, 1999, 99: 243–248
52 Li W, Li Q, Liu S, Duan C, Ying L, Huang F, Cao Y. *Sci China Chem*, 2015, 58: 257–266
53 Sun D, Meng D, Cai Y, Fan B, Li Y, Jiang W, Huo L, Sun Y, Wang Z. *J Am Chem Soc*, 2015, 137: 11156–11162
54 Blom PWM, Mihailetchi VD, Koster LJA, Markov DE. *Adv Mater*, 2007, 19: 1551–1566
55 Fan B, Ying L, Wang Z, He B, Jiang XF, Huang F, Cao Y. *Energy Environ Sci*, 2017, 10: 1243–1251